
Multi-AGV Path Planning Method via Reinforcement Learning and Particle Filters

Shao Shuo

Wuhan University of Technology

shaoshuo@whut.edu.cn

Abstract

The Reinforcement Learning (RL) algorithm, renowned for its robust learning capability and search stability, has garnered significant attention and found extensive application in Automated Guided Vehicle (AGV) path planning. However, RL planning algorithms encounter challenges stemming from the substantial variance of neural networks caused by environmental instability and significant fluctuations in system structure. These challenges manifest in slow convergence speed and low learning efficiency. To tackle this issue, this paper presents the Particle Filter-Double Deep Q-Network (PF-DDQN) approach, which incorporates the Particle Filter (PF) into multi-AGV reinforcement learning path planning. The PF-DDQN method leverages the imprecise weight values of the network as state values to formulate the state space equation. Through the iterative fusion process of neural networks and particle filters, the DDQN model is optimized to acquire the optimal true weight values, thus enhancing the algorithm's efficiency. The proposed method's effectiveness and superiority are validated through numerical simulations. Overall, the simulation results demonstrate that the proposed algorithm surpasses the traditional DDQN algorithm in terms of path planning superiority and training time indicators by 92.62% and 76.88%, respectively. In conclusion, the PF-DDQN method addresses the challenges encountered by RL planning algorithms in AGV path planning. By integrating the Particle Filter and optimizing the DDQN model, the proposed method achieves enhanced efficiency and outperforms the traditional DDQN algorithm in terms of path planning superiority and training time indicators.

1 Introduction

Due to its significant role and wide application prospects in both military and civilian domains, the Autonomous Guided Vehicle (AGV) has gained considerable attention in the field of robotics [1]. Path planning, which is essential for achieving AGV intelligence, has also attracted extensive research interest [2]. Broadly speaking, AGV path planning algorithms can be categorized into two types: traditional algorithms and population-based intelligent optimization algorithms.

Traditional path planning methods, such as graphical methods [3], artificial potential field methods [4], and dynamic window approaches [5], offer the advantage of short planning time. However, they suffer from deficiencies in planning stability and adaptability. On the other hand, artificial intelligence optimization algorithms, including genetic algorithms [6], neural networks [7], and ant colony algorithms [8], can achieve stable planning in complex environments due to their population-based characteristics [9].

One of the most prominent population-based intelligent optimization algorithms is Reinforcement Learning (RL), which exhibits powerful machine learning capabilities and enables the intelligent agent to learn specific behavioral norms through trial and error [10]. Moreover, this algorithm

possesses the characteristics of reward-based feedback and does not rely on training data, making it naturally adaptable in the field of path planning [11].

Reinforcement Learning is an influential machine learning approach that enables intelligent agents to acquire knowledge on how to act within an environment to accomplish predefined objectives through reward feedback. It does so without any prior understanding of the environment or training data [12]. This characteristic makes it especially well-suited for tasks related to local path mapping. Double Deep Q-Network (DDQN) represents a renowned RL algorithm that has gained extensive utilization in the field of path planning.

However, AGV planning remains challenging for current Deep Reinforcement Learning (DRL) methods, partly due to their need to (i) reason in partially observable environments and (ii) reason through complex observations, such as avoiding collisions between AGVs. While most existing RL path planning algorithms have shown feasibility in single AGV path planning problems, they fail to achieve multi-AGV path planning in more complex environments. This is because the neural networks have high variance, leading to slow convergence of the algorithm and reducing its ability to handle cooperative planning among multiple agents in complex environments [13].

In light of this, some studies have proposed improvements to the algorithm by increasing the complexity of the grid state space and incorporating perception state space [14]. However, this method still relies on training results in an ideal noise-free environment, resulting in the inability to address the issue of weight inaccuracy [15]. It is feasible to overcome these constraints; however, doing so incurs supplementary computational expenses when training deep neural networks. Additionally, some research has aimed to improve DRL algorithms by introducing Kalman filtering [16]. However, traditional Kalman filters require linearization of the model through Taylor series, which compromises the accuracy of the model to some extent.

Within this study, we explore the path planning of AGVs in an unfamiliar environment, considering multiple designated destinations. In typical scenarios, intricate tasks involving mobile robots, such as mapping, item delivery, or surveillance, necessitate path planning for multiple targets. Our conjecture is that the conventional DDQN approach fails to address the challenge of path planning for multiple targets due to the convergence of Q-values solely based on the spatial coordinates on the map. Empirical findings illustrate that while DDQN can successfully learn to plan a path for the initial target, it struggles to efficiently plan for subsequent targets due to the environment's complexity and the incapability to learn and regenerate the value network for the remaining targets. Despite researchers' efforts to modify DDQN and reduce convergence time, there is currently no existing research on employing Particle Filter (PF) integration to tackle the issue of multi-AGV path planning within this environment. The subsequent section will provide a more comprehensive explanation of the DDQN algorithm.

To address the aforementioned issues, this paper proposes a PF-DDQN-based method for multi-AGV path planning. Firstly, in the proposed method, the training network with environmental noise and the target network with inaccurate weights are treated as state and observation variables, respectively, to construct the system's state equation and observation equation. Then, through the fusion iteration of neural networks and particle filters, the weights of the neural network are continuously updated to improve the convergence speed of the proposed algorithm. Finally, the effectiveness and superiority of the proposed method are validated through numerical simulations under different operating conditions.

The structure of the remaining part of this paper is as follows: Section 2 introduces related work, Section 3 presents the theoretical background of methods, Section 4 compares the experimental results of the proposed algorithm with DDQN and EKF-DDQN. Finally, Section 5 provides a summary of this paper.

2 Related Work

Genetic Algorithms (GAs) and Ant Colony Optimization (ACO) are heuristic methods that show potential in solving optimization problems [17]. GAs generate a collection of potential solutions through Darwinian evolution principles and assess them using a fitness function. The fittest individuals are selected for reproduction through crossover operations, while population diversity is maintained through mutation operations [18]. Conversely, ACO draws inspiration from the behavior of ants

and utilizes pheromone trails to improve the efficiency of the shortest paths between initial and final points [19].

In recent years, researchers have proposed various optimization techniques for path planning of mobile robots in grid environments. Li et al. [20] introduced an enhanced algorithm called Improved Ant Colony Optimization-Improved Artificial Bee Colony (IACO-IABC), which effectively improves the performance of mobile robot path planning by combining the strengths of both algorithms and introducing new heuristics and search mechanisms. Li et al. [21] proposed an advanced Ant Colony Optimization (MACO) algorithm that addresses issues such as local optima and slow convergence in trajectory planning for Unmanned Aerial Vehicles (UAVs) by incorporating the metropolis criterion and designing three trajectory correction schemes. Additionally, they employed an Inscribe Circle (IC) smoothing method to enhance efficiency and safety in trajectory planning.

While GAs and ACO have emerged as solutions for path planning problems, their effectiveness in real-time path planning is limited. These population-based algorithms are computationally demanding, particularly for large search spaces, making them unsuitable for real-time applications that require prompt decision-making. Furthermore, the population-based approaches employed by these algorithms can yield suboptimal solutions and exhibit slow convergence, especially in complex environments [22].

The Double Deep Q-Network (DDQN) algorithm has gained significant traction in the field of reinforcement learning for acquiring optimal action sequences based on a predefined policy. This algorithm is renowned for its simplicity, speed, and effectiveness in addressing challenging problems in complex and unknown environments. Numerous researchers have applied the DDQN algorithm to path planning by discretizing real-world scenarios into a state space and subsequently simulating them. These methods differ in terms of task-specific behavior design and the representation of the state space.

One of the earliest approaches was the Deep Q-Network (DQN) algorithm proposed by Mnih et al. [23], which combines deep neural networks with Q-learning to address reinforcement learning problems in high-dimensional and continuous state spaces. The DQN algorithm resolves the instability issue in Q-learning by employing an experience replay buffer and a target network.

To address the overestimation problem in the DQN algorithm, Hasselt et al. [24] introduced the use of two Q-networks: one for policy action selection and the other for action value estimation. They utilized a target value network to alleviate the overestimation problem and improve training stability. They also introduced distributed reinforcement learning, modeling the value of actions as probability distributions rather than single values. The use of quantile regression to estimate the distribution of action values enhances learning efficiency and stability [25].

Igl et al. [26] adopted the Variational Sequential Monte Carlo method, while Naesseth et al. [27] applied particle filters for belief tracking in reinforcement learning. The latter method enhances belief tracking capability, but experiments reveal that generative models lack robustness in complex observation spaces with high-dimensional uncorrelated observations. To address this issue, more powerful generative models such as DRAW [28] can be considered to improve observation generation models. However, evaluating complex generative models for each particle significantly increases computational costs and optimization difficulty.

Recent attention has focused on embedding algorithms into neural networks for end-to-end discriminative training. This idea has been applied to differentiable histogram filters, such as Jonschkowski & Brock [29], and Kalman filters [30]. Ma et al. [31] integrated particle filters with standard RNNs (e.g., LSTM) and introduced PF-RNN for sequence prediction.

Muruganantham et al. [32] proposed a dynamic Multi-Objective Evolutionary Algorithm (MOEA) based on Extended Kalman filter (EKF) prediction. These predictions guide the search for changing optima, accelerating convergence. A scoring scheme was designed to combine EKF prediction with random reinitialization methods to enhance dynamic optimization performance.

Gao et al. [33] presented an adaptive Kalman filter navigation algorithm, RL-AKF, which employs reinforcement learning methods to adaptively estimate the process noise covariance matrix. Extensive experimental results demonstrate that although this algorithm accurately estimates the process noise covariance matrix and improves algorithm robustness, it is time-consuming and faces convergence challenges.

In this work, we depart from directly combining particle filters and RL algorithms. Instead, building upon previous work, we treat the weightsof the neural network as state variables in the particle filter algorithm. We leverage the highly adaptive and nonlinear iterative characteristics of particle filters to update the network weights, reducing the variance of the target network in the RL algorithm. This approach enhances the accuracy of action guidance for trajectories and improves the convergence speed of the reinforcement learning algorithm.

3 Methods

3.1 Particle Filtering

PF is a recursive Bayesian filtering algorithm utilized for state estimation within a system. Its core principle involves approximating the probability distribution $p(x_k|z_{1:k})$ by employing a set of random samples, known as particles, which represent the states [18]. Here, let $x_{0:k} = x_0, x_1, \dots, x_k$ and $z_{0:k} = z_0, z_1, \dots, z_k$ represent the target states and observed values at time k . The particle weight update function depends on the target states and observation data $x_{i,k} \sim q(x_{i,k} | x_{i,k-1}, z_k)$, which can be expressed as follows:

$$w_k^i = \frac{p(z_k|x_k^i)p(x_k^i|x_{k-1}^i)}{q(x_k^i|x_{k-1}^i, z_k)} \cdot w_{k-1}^i \quad (1)$$

Consequently, a collection of particles with weight values $x_k^i, w_{k-1}^i, \dots, x_k^N, w_k^N$ approximates the posterior probability density, where the importance sampling function is defined as follows:

$$q\left(\frac{x_k^i}{x_{k-1}^i z_k}\right) = p\left(\frac{x_k^i}{x_{k-1}^i}\right) \quad (2)$$

The PF algorithm follows the subsequent steps:

Step 1: Sample $x_{i,k} \sim q(x_{i,k}|x_{i,k-1}, z_k)$ for $i = 1, \dots, N_s$.

Step 2: Calculate the importance weight \tilde{w}_k^i , normalize it, and update particle weights.

Step 3: Compare the effective sample size \tilde{N}_{eff} with a predefined threshold N_{th} . If $\tilde{N}_{\text{eff}} < N_{\text{th}}$, perform resampling of $(x_k^i, w_k^i)_{i=1}^{N_s}$.

Unlike the conventional Kalman filter, particle filtering is not reliant on linearization or Gaussian assumptions, making it more suitable for the iterative updating of neural networks [19].

3.2 Extended Kalman Filtering

The Extended Kalman Filter (EKF) is an extension of the Kalman Filter that addresses the estimation of system states in the presence of nonlinear system dynamics and measurement models. It approximates the nonlinear models using linearization techniques and applies the EKF update equations to iteratively estimate the state of the system.

Similar to the Kalman Filter, the EKF maintains an estimate of the system state, denoted as \hat{x}_k , and an error covariance matrix, denoted as P_k , which represents the uncertainty associated with the estimate. The EKF incorporates new measurements to update the state estimate and the error covariance matrix.

The EKF consists of two main steps: the prediction step and the update step.

Prediction Step: In the prediction step, the EKF predicts the current state based on the previous estimate and the nonlinear system dynamics. It updates the estimate of the state and the error covariance matrix using the following equations:

$$\hat{x}_k^- = f(\hat{x}_{k-1}, u_{k-1}) \quad (3)$$

$$P_k^- = F_k P_{k-1} F_k^T + Q_k \quad (4)$$

where \hat{x}_k^- and P_k^- are the predicted state estimate and the predicted error covariance matrix, respectively. The function $f(\cdot)$ represents the nonlinear system dynamics, and u_{k-1} is the control input at time step $k-1$. The matrix F_k is the Jacobian matrix of the system dynamics function evaluated at the predicted state, and Q_k is the process noise covariance matrix that represents the uncertainty in the system dynamics.

Update Step: In the update step, the EKF incorporates the new measurement to improve the estimate of the state. It computes the Kalman gain, which determines the weight given to the measurement and the predicted state estimate, and updates the state estimate and the error covariance matrix using the following equations:

$$K_k = P_k^- H_k^T (H_k P_k^- H_k^T + R_k)^{-1} \quad (5)$$

$$\hat{x}_k = \hat{x}_k^- + K_k (z_k - h(\hat{x}_k^-)) \quad (6)$$

$$P_k = (I - K_k H_k) P_k^- \quad (7)$$

where K_k is the Kalman gain, H_k is the Jacobian matrix of the measurement function evaluated at the predicted state, R_k is the measurement noise covariance matrix, and z_k is the measurement obtained at time step k . The function $h(\cdot)$ represents the measurement model that relates the true state to the measurements.

The EKF linearizes the nonlinear system dynamics and measurement models using the Jacobian matrices. By approximating them as linear, the EKF can apply the Kalman Filter update equations to estimate the state. However, the linearization introduces errors, and the accuracy of the EKF depends on the quality of the linearization. In cases where the nonlinearities are significant, more advanced techniques like the Unscented Kalman Filter or Particle Filter may be more appropriate for state estimation.

3.3 Double Deep Q-network Algorithm

The DDQN algorithm is an enhanced iteration of the Deep Q-Network (DQN) algorithm [21]. In contrast to conventional methods with similar objectives, DDQN mitigates the adverse effects of overestimation by employing the current estimation network to approximate the maximum Q-value of the subsequent state, rather than relying solely on the target network [23]. Within the DDQN algorithm, a target network architecture is established to minimize the loss function, which can be mathematically expressed as follows:

$$L(\theta) = \frac{1}{2} \sum_i (Q(s_i, a_i; \theta) - y_i)^2 \quad (8)$$

Where, y_i represents the target Q-value, and $Q(s_i, a_i; \theta)$ represents the predicted Q-value. The network is trained using stochastic gradient descent to update the network weights θ at each time-step i , resulting in improved estimates of the Q-values. The update expression of the Q-value is shown in Equation:

$$Q(s_i, a_i; \theta) = r_t + \gamma \max Q(s_{t+1}, a_{t+1} | \tilde{\theta}) \quad (9)$$

Where, r_t represents the reward value obtained from the corresponding action at time t , while γ denotes the discount factor. The derivative of the loss function with respect to the network parameters θ , in terms of γ , is expressed as following Equation:

$$\nabla_{\theta} L(\theta) = \sum_i (Q(s_i, a_i, \theta) - y_i) \nabla_{\theta} Q(s_i, a_i; \theta) \quad (10)$$

At this juncture, the update rule for the weights is defined as illustrated in following Equation:

$$\theta_{t+1} = \theta_t + \alpha (Z_t - Q(s_t, a_t; \theta)) \frac{dQ(s_t, a_t; \theta)}{d\theta_t} \quad (11)$$

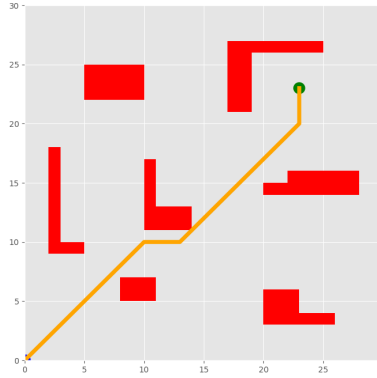


Figure 1: The 2D map of AGV path planning

Where, θ_t represents the network weights at the current moment, while θ_{t+1} denotes the updated network weights. α signifies the learning rate, which governs the step size of weight updates. Z_t represents the value of the target network's value function for the current state and action [25].

The DDQN algorithm improves convergence speed and addresses overestimation issues in traditional DQN algorithms. However, it still faces challenges in effectively addressing weight inaccuracy within the model, which limits its superiority. To overcome these limitations, this study introduces a novel algorithm called PF-DDQN, which combines PF and DDQN.

3.4 Simulation Environment Modeling

The environment is a 2D map as shown in Figure 1, represented as a 30×30-pixel image, where each pixel corresponds to a 2-meter size in the real world. The training utilizes an entirely unfamiliar map, which is a 30×30-pixel image. In this image, the red and white regions correspond to obstacles and free space, respectively. The trajectory of the AGV and the target are depicted by different colors, with the former represented by colors other than green. Since the mobile robot lacks knowledge of the reference map, it is imperative for it to generate its own map.

The goal of AGV spatial trajectory planning is to achieve collision-free detection for the AGV. Therefore, during spatial trajectory planning, optimization of the trajectory is required based on two aspects: the relationship between the AGV and obstacle positions and the relative position between the AGV and obstacles.

Real AGVs rely on vision to determine their position. In this work, the three-dimensional position parameters of the target are obtained through trigonometry and disparity. Given the relative positioning between two cameras and the internal parameters of the cameras, the spatial coordinates or dimensions of an object can be obtained by knowing the disparity of its features. The coordinate system of the environmental image is shown in Figure 2.

As depicted in Figure 2, a u-v-o Cartesian coordinate system is defined in the obtained image, where the pixel coordinates correspond to the rows and columns in the sequence. Therefore, (u, v) represents the pixel coordinate system of the AGV.

Since (u, v) only indicates the number of rows and columns where the pixel is located, in order to describe the position of the pixel in the image, an equivalent meaning needs to be established using a physical coordinate system. Thus, a coordinate system parallel to the (u, v) axis is established, with the x-axis corresponding to the u-axis and the y-axis corresponding to the v-axis. (u, v) corresponds to (x, y) .

The coordinates are expressed in pixels and correspond to the image's coordinate system, which is measured in millimeters. Thus, the relationship between the position of any pixel in the image and the two coordinate systems can be described as follows:

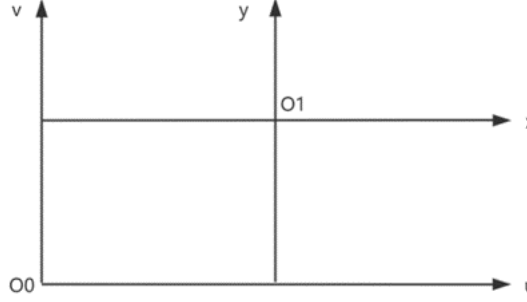


Figure 2: **Graph environment image coordinate system**

$$\begin{cases} u = \frac{x}{dx} + u_0 \\ v = \frac{y}{dy} + v_0 \end{cases} \quad (12)$$

The position of the overlap point between the camera optical axis and the image plane in the xy coordinate system is denoted as (u_0, v_0) . By transforming the equation into homogeneous coordinates and matrix form, we can obtain:

$$\begin{bmatrix} u \\ v \\ 1 \end{bmatrix} = \begin{bmatrix} \frac{1}{dx} & 0 & u_0 \\ 0 & \frac{1}{dy} & v_0 \\ z & 0 & 1 \end{bmatrix} \quad (13)$$

Where, z represents the state vector of the matrix. The inversion is as follows:

$$\begin{bmatrix} x \\ y \\ 1 \end{bmatrix} = \begin{bmatrix} dx & 0 & -u_0 dx \\ 0 & dy & -v_0 dy \\ 0 & 0 & 1 \end{bmatrix} \begin{bmatrix} u \\ v \\ 1 \end{bmatrix} \quad (14)$$

When a camera captures an object, there exists a unique projection relationship between the object's true coordinates and the obtained image coordinates [8]. Given the knowledge of the camera's geometric parameters, the principle of similar triangles can be used to derive:

$$\begin{cases} u = \frac{f}{-z_e} x_e \\ v = \frac{f}{-z_e} y_e \end{cases} \quad (15)$$

Where, $-Z_e$ represents the camera depth, and $f / -Z_e$ represents the scale factor. Perspective projection only guarantees a one-to-one correspondence between points on the image and points on the projection line. In other words, the same point on the image corresponds to a series of points on the projection line. It is evident that during this process, the depth information of the spatial points is lost, which indicates the need for two or more cameras to determine the three-dimensional object. By calculating the image coordinates, the position of a three-dimensional point in the camera coordinate system can be obtained:

$$\begin{cases} x_e = \frac{f}{f+w} u \\ y_e = \frac{f}{f+w} v \\ z_e = \frac{f^2}{f+w} \end{cases} \implies \begin{cases} x_e = \frac{-z_e}{f} u \\ y_e = \frac{-z_e}{f} v \\ z_e = z_e \end{cases} \quad (16)$$

Where, z_e is related to the true distance between the target and the camera. Therefore, this experiment can achieve the conversion from 3D to 2D.

The working scenario designed in this paper is as follows: In a complex work space with great danger, multiple AGVs cooperate with each other to jointly select the best path according to the coordinates of obstacles and target points. In order to improve the likelihood of an AGV successfully executing its task, the robot-generated path needs to meet the following conditions:

- (a) After the AGV is started, problems such as insufficient power and sudden failure are ignored;
- (b) The paths generated by each AGV need to be collision free from obstacles;
- (c) The paths generated between each AGV should be collision-free;
- (d) The generated path must ensure that the robot reaches its destination at the same time.
- (e) Assume that the speed of each robot i is bounded by $[V_{min}^i, V_{max}^i]$, where V_{min}^i and V_{max}^i represent the minimum and maximum speed of robot i , respectively. As the robot navigates to the target location, the speed of each robot varies within its velocity boundary.
- (f) During the movement of each AGV to the target position, the yaw Angle and travel distance of each AGV need to be kept within its maximum yaw Angle and distance constraints, respectively.

In this experiment, we consider the total path length of the multi-AGV system as the global objective function for the path planning problem. The total path length is defined as the sum of the path lengths of each AGV. Mathematically, the objective function is represented as follows:

$$F = \min \left\{ \sum_{i=1}^m L_i \right\} \quad (17)$$

Here, the variable m represents the total number of AGVs, and L_i represents the planned path length of the i -th AGV. The path length of each AGV, L_i , can be calculated using the following formula:

$$L_i = \sum_{k=0}^{ns} \text{dis}(p_{i,k}, p_{i,k+1}) \quad (18)$$

We define $p_{i,0}$ and $p_{i,ns+1}$ as the initial and final positions of the i -th robot, respectively. The term $\text{dis}(p_{i,k}, p_{i,k+1})$ represents the Euclidean distance between waypoints $p_{i,k}$ and $p_{i,k+1}$. The path for the i -th robot is denoted as $\text{path}_i = [p_{i,0}, p_{i,1}, \dots, p_{i,ns}, p_{i,ns+1}]$, where $\text{path}_{i,k}$ ($k = 0, 1, \dots, n+l$) represents the k -th waypoint along the path generated by the i -th robot.

The yaw angle, $\theta_{i,k}$, of the i -th robot at the k -th path segment along the generated path is computed using the following equation:

$$\theta_{i,k} = \arccos \left[\frac{(x_{i,k+1} - x_{i,k})(x_{i,k+2} - x_{i,k+1}) + (y_{i,k+1} - y_{i,k})(y_{i,k+2} - y_{i,k+1})}{\text{dis}(p_{i,k}, p_{i,k+1}) \cdot \text{dis}(p_{i,k+2}, p_{i,k+1})} \right] \quad (19)$$

The path planning problem is subject to the following constraints:

$$\begin{cases} L_i^{\min} \leq L_i \leq L_i^{\max} \\ \theta_i^{\min} \leq \theta_{i,k} \leq \theta_i^{\max}, \quad 1 \leq k \leq ns \\ p_{i,k} p_{i,k+1} \cap \text{obstacle} \in \text{null}, \quad 0 \leq k \leq ns \\ \text{path}_i \cap \text{path}_j \in \text{null}, \quad \forall i \neq j, i, j \in N \\ T_i \cap T_j \cap \dots \cap T_N \notin \text{non-null} \end{cases} \quad (20)$$

Here, L_i^{\min} and L_i^{\max} represent the minimum and maximum path length constraints for the i -th robot, respectively. θ_i^{\min} and θ_i^{\max} represent the minimum and maximum constraints for the yaw angle rotation of the i -th AGV. T_i is the arrival time for the i -th robot at the destination position. The variables $x_{i,k}$ and $y_{i,k}$ represent the values of the AGV on the x and y axes, respectively. The term "obstacle" indicates the position coordinate of the obstacle. The term "null" defines the path intersection between any two different robots at the same time as an empty set, ensuring collision-free

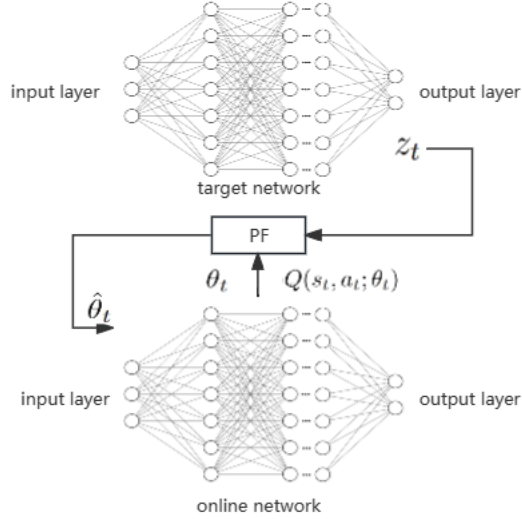


Figure 3: **DDQN and PF combined structure.**

paths between any AGV and the obstacle. The term "non-null" indicates that the intersection of the arrival times of any two different AGVs is a non-empty set, implying that the paths generated by different AGVs can ensure simultaneous arrival at the destination.

3.5 PF-DDQN Algorithm

This article proposes the PF-DDQN algorithm, which employs PF to address the issue of weight inaccuracy in deep reinforcement learning models. The algorithm's structure is depicted in Figure 3.

In the proposed algorithm, the state equation and observation equation, which describe the dynamics of the system, are assumed to be represented as follows:

$$\begin{aligned} x_t &= f(x_{t-1}) + w_{t-1} \\ z_t &= h(x_t) + v_t \end{aligned} \quad (21)$$

Where, x_t represents the state vector, z_t represents the measurement vector, $f(x_{t-1})$ signifies the state transition function, $h(x_t)$ denotes the transfer function between the state and observation vectors, w_{t-1} represents the process noise, and v_t represents the observation noise.

Subsequently, the weight parameters $θ_t$, z_t , and $Q(s_t, a_t; θ_t)$ corresponding to time t are substituted into the PF state equation and observation equation, as represented by the following equations:

$$\begin{aligned} θ_t &= θ_{t-1} + W_{t-1} \\ Z_t &= Q(s_t, a_t; θ_t) + v_t \end{aligned} \quad (22)$$

Let $t - 1$ time have a set of posterior particles, expressed as:

$$\{x_{t-1}(i), ω_{t-1}(i); i = 1, 2, \dots, N\} \quad (23)$$

Where, N represents the number of particles, $x_{t-1}(i)$ denotes the i -th particle at time $t - 1$, and $ω_{t-1}(i)$ signifies the weight of the i -th particle at time $t - 1$.

The entire algorithm flow is described as follows:

Particle set initialization, $t = 0$: Random samples are drawn from the prior probability density $p(θ_0)$, denoted as $θ_0(1), θ_0(2), \dots, θ_0(N)$ (where N represents the number of random samples).

When $t = 1, 2, \dots$, perform the following steps: (a) State prediction:

The prior particles at time step k are drawn based on the system's state equation, as shown in the following equation:

$$\{\theta_{t|t-1}(i); i = 1, 2, \dots, N\} \sim p(\theta_k | \theta_{k-1}) \quad (24)$$

(b) Update:

First, the weight update is performed. After obtaining the measured values of the neural network weights, the particle weights, denoted as $w_t^{(j)}$, are calculated based on the system's observation equation, as shown in the following equation:

$$\omega_t^{(i)} = \omega_{t-1}^{(i)} p(Z_t | \theta_t^{(i)}), \quad i = 1, \dots, N \quad (25)$$

Then, calculate the number of effective particles \tilde{N}_{eff} , and compare it with the set threshold N_{th} . If $\tilde{N}_{eff} < N_{th}$, then resample the prior particle set to obtain N particles of equal weight. Otherwise, proceed to the next step.

(c) Estimation:

After iterating t times, the true parameter estimation $\hat{\theta}_t$ is obtained and returned to the estimation network for value function computation. The specific formula is given by the following equation:

$$\hat{\theta}_t = \sum_{i=1}^N \theta_{t|t-1}(i) \omega_t^{(i)} \quad (26)$$

The fundamental particle filtering algorithm maintains the past samples unchanged when sampling at time step t , and the importance weights are iteratively computed. In summary, the combination of particle filtering and double deep Q-network involves the following steps:

Step 1: Utilizing the DDQN model, the parameters $\theta_t, Q(s_t, a_t; \theta)$, and z_t at time t are employed as inputs to construct the state equation and observation equation for the PF. Furthermore, the particle set is initialized.

Step 2: Iteratively updating, performing state prediction, weight updating, and resampling operations at each time step to obtain the optimal estimation of true weights $\hat{\theta}_t$.

Step 3: Transmitting the optimal true parameters $\hat{\theta}_t$ to the estimation network to obtain $Q(s_t, a_t; \theta)$, which is used to select the action corresponding to the maximum Q-value during experience exploitation, thereby enhancing the accuracy of the neural network's application in the DDQN algorithm. After obtaining θ_{t+1} , Z_{t+1} , and $Q(s_{t+1}, a_{t+1}; \theta)$ at time $t+1$, the above process is repeated to obtain the optimal decision for the next step, cycling through this process until the model converges.

3.5.1 Status and Reward Mechanisms

The path planning method for multi-AGV based on PF-DDQN considers each AGV as an intelligent agent, where its position on the grid map is regarded as the controlled object. The actions of the AGV correspond to its movements, and the intelligent agent selects an action based on the current state, executes it, and observes the resulting state and reward. The agent continuously updates its parameters to maximize the reward until the optimal action is determined.

The algorithm framework is shown in Figure 4. The algorithm employs an experience pool to store previous training memories, which aids in the training of the DDQN network. In the framework, θ represents the network weights at time t , r represents the reward at time t , (s, a, r, s') represents the replay memory unit at time t , s represents the state at time t , and a represents the action at time t .

3.5.2 State Space and Action Space

In order to accurately represent the operating environment of the AGV and facilitate the training process, this study adopts a grid-based approach to depict the entire working area. Each grid is

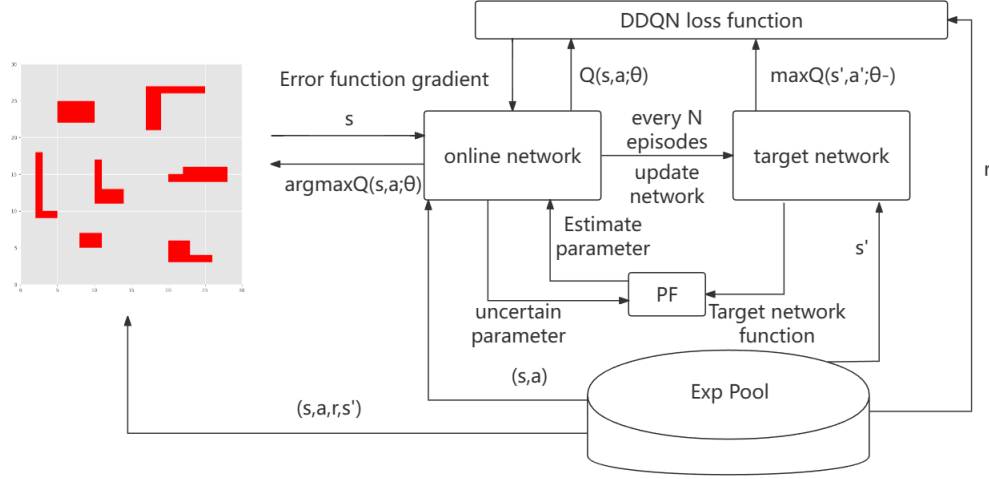


Figure 4: **Overall framework of the PF-DDQN model.**

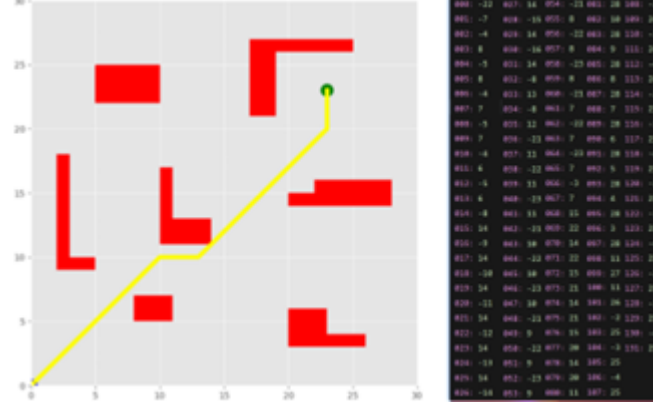


Figure 5: **Overall planning environment and path diagram.**

divided into $2 \times 2m$ sizes, which corresponds to the length of the AGV. The state variables of the AGV include its relative positions to obstacles and target points. In terms of planning, the AGV has nine possible actions: northward, southward, eastward, westward, northeastward, southeastward, northwestward, southwestward, or remaining stationary. Figure 5 illustrates the overall planning environment and the path diagram.

3.5.3 Reward Function

The reward function plays a critical role in reinforcement learning as it guides the learning process of the intelligent agent and influences action selection. Therefore, appropriately defining rewards is essential to achieve desired outcomes and optimal action strategies. In the context of multi-AGV path planning, the primary objective is to minimize the total trajectory points traversed by each AGV while successfully reaching their target points. In this study, the reward is defined with four components:

Baseline Value: To decrease the overall trajectory count, a penalty value of -4 is assigned when an AGV takes an action to change its position.

Distance to Target Point: When the sum of distances between all AGVs and their target points decreases, indicating progress, a reward of 5 is assigned. Conversely, a penalty of -5 is given when distances increase. Reward 200 when it overlaps with the target point.

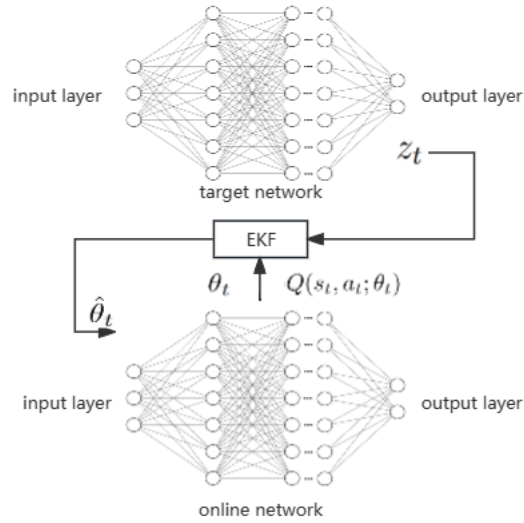


Figure 6: **DDQN and EKF combined structure.**

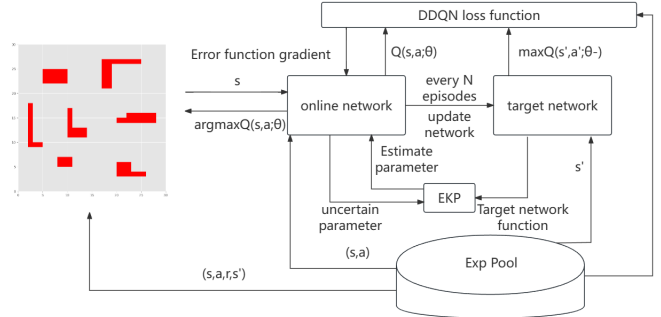


Figure 7: **Overall framework of the EKF-DDQN model.**

Distance to Obstacle: To ensure obstacle avoidance, an AGV is penalized with a value of -20 if it collides with an obstacle.

Distance between AGVs: Rewards are assigned based on the distances between AGVs. Only when AGVs collide, a penalty of -20 is imposed, treating other AGVs as obstacles. This reward and penalty mechanism is independent of the distances between the AGVs.

3.6 EKF-DDQN Algorithm

Similar to PF-DDQN, we can also replace PF with EKF, combine EKF with neural network, and update network weights according to the update mode of EKF. The algorithm structure is shown in Figure 6, The algorithm framework is shown in Figure 7.

In the EKF-DDQN algorithm, the state equation and observation equation, which describe the dynamics of the system, are assumed to be represented as follows:

$$x_t = f(x_{t-1}, u_{t-1}) + w_{t-1} \quad (27)$$

$$z_t = h(x_t) + \nu_t \quad (28)$$

Where, x_t represents the state vector, z_t represents the measurement vector, $f(x_{t-1}, u_{t-1})$ signifies the nonlinear state transition function, $h(x_t)$ denotes the measurement function, w_{t-1} represents the process noise, and ν_t represents the measurement noise.

To update the parameter vector θ using the EKF, the following EKF update equations are employed:

$$\theta_t^- = \theta_{t-1} \quad (29)$$

$$P_t^- = F_{t-1} P_{t-1} F_{t-1}^T + Q_{t-1} \quad (30)$$

$$K_t = P_t^- H_t^T (H_t P_t^- H_t^T + R_t)^{-1} \quad (31)$$

$$\theta_t = \theta_t^- + K_t (z_t - h(\theta_t^-)) \quad (32)$$

$$P_t = (I - K_t H_t) P_t^- \quad (33)$$

Where, θ_t^- and P_t^- represent the predicted parameter estimate and the predicted error covariance matrix, respectively. F_{t-1} and H_t are the Jacobian matrices of the state transition function and the measurement function evaluated at the predicted parameter estimate, while Q_{t-1} and R_t are the process noise covariance matrix and the measurement noise covariance matrix, respectively.

The EKF-DDQN algorithm follows a similar flow to the PF-DDQN algorithm, with the following modifications:

EKF-DDQN Algorithm:

Initialization, $t = 0$: Set an initial estimate for the parameter vector θ_0 based on prior knowledge or assumptions.

When $t = 1, 2, \dots$, perform the following steps: (a) State prediction:

Obtain the predicted parameter estimate at time step t using the system's state equation and the EKF prediction equations:

$$\theta_t^- = f(\theta_{t-1}, u_{t-1}) \quad (34)$$

$$P_t^- = F_{t-1} P_{t-1} F_{t-1}^T + Q_{t-1} \quad (35)$$

(b) Update:

Incorporate the new measurement z_t to improve the parameter estimate using the EKF update equations:

$$K_t = P_t^- H_t^T (H_t P_t^- H_t^T + R_t)^{-1} \quad (36)$$

$$\theta_t = \theta_t^- + K_t (z_t - h(\theta_t^-)) \quad (37)$$

$$P_t = (I - K_t H_t) P_t^- \quad (38)$$

The remaining steps of the algorithm, including weight updating and resampling, remain unchanged.

The algorithm iteratively performs state prediction and update steps, resulting in an optimized estimate of the true weights θ_t . These optimized weights are then used to compute the value function $Q(s_t, a_t; \theta)$, which is utilized in the decision-making process to select the action corresponding to the maximum Q-value during experience exploitation. The algorithm continues to iterate, updating θ_{t+1} , z_{t+1} , and $Q(s_{t+1}, a_{t+1}; \theta)$ in each iteration.

4 Experiment Setup and Results

The numerical simulations in this study were conducted on a system comprising an Intel Core i7-6500 3.20GHz processor, a GPU GTX 3060 with 6GB of memory, and 8GB of RAM. The simulations were performed on both the Ubuntu 20.04 and Windows 11 operating systems using Python.

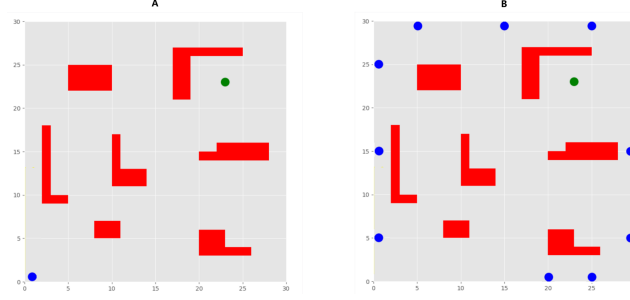


Figure 8: **Training maps for A) experiments 1 and B) experiment 2, where the robot start point, targets, obstacles, and free space are represented as blue, green, magenta, and white.**

This section validates the proposed PF-DDQN path planning algorithm's superior convergence speed and performance compared to the traditional DDQN and EKF-DDQN algorithms through experimental verification. Two simulation experiments are conducted to train PF-DDQN, DDQN, and EKF-DDQN. As illustrated in Figure 8, Experiment 1 focuses on the path planning of a single AGV to a fixed target, where the AGV starts from the initial position and aims to reach a fixed target without colliding with obstacles. Experiment 2 involves the path planning of multiple AGVs to a fixed target, where multiple AGVs start from dispersed initial positions and aim to reach a fixed target without colliding with obstacles or each other. In the same unknown environment and under identical conditions, quantitative and qualitative comparisons are made among PF-DDQN, DDQN, and EKF-DDQN by evaluating their results using the same set of parameters.

In the simulation experiments, the parameters of the deep reinforcement learning network are presented in Table 1.

Table 1: System Parameters

Parameter	Value
Memory size	10000
Batch size	500
Discount factor	0.95
Learning rate	0.0001
Model update frequency	50
Initial exploration rate	1.0
Exploration rate decay	0.9995
Final exploration rate	0.001

4.1 Experiment 1: Path Planning Comparison for a Single AGV

In this experiment, the PF-DDQN, EKF-DDQN, and DDQN algorithms underwent 60,000 training iterations. The AGV started from the bottom-left corner of the map and navigated through seven clusters of obstacles to reach a fixed position in the upper-right corner.

Figure 9 depicts the paths planned by the three methods. It is evident from the figure that all three algorithms successfully guide the AGVs to their target points, with similar path lengths. This indicates the feasibility and stability of the algorithms.

The learning curves of the three methods are illustrated in Figure 10. The experimental results demonstrate that the PF-DDQN and EKF-DDQN methods, which incorporate filters, exhibit similar convergence speeds and yield consistent trajectories. In comparison, they outperform the traditional DDQN algorithm by achieving faster and more efficient solutions.

The DDQN algorithm provides the shortest path from the starting point to the target point, assuming prior knowledge of the map layout. However, in real industrial environments, the behavior of AGVs

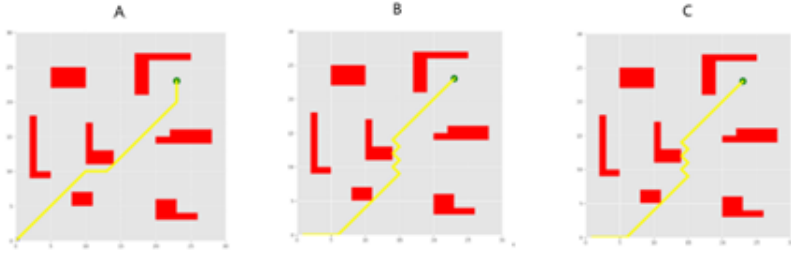


Figure 9: **Final path results of the experiment for single AGV: A) DDQN, B) EKF-DDQN, and C) PF-DDQN after path smoothing for 60,000 episodes.**

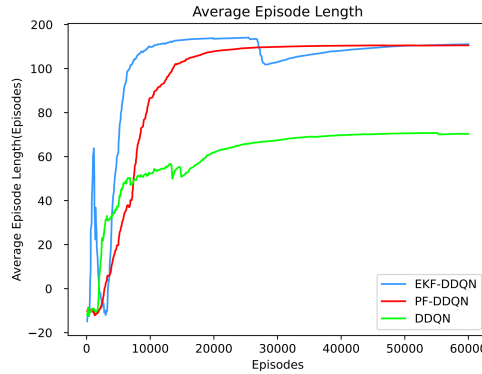


Figure 10: **Learning curves for single-AGV target path planning: Comparison of the proposed method with EKF-DDQN and DDQN after training.**

near obstacles can be hazardous. As the reward function influences path planning behavior, the PF-DDQN method prioritizes safety by better avoiding obstacles, even if it results in a slightly longer path.

Table 2 presents the specific numerical simulation results of this experiment. Compared to the DDQN algorithm, the proposed method in this study reduced the overall training time by 20.69% over 60,000 iterations. Additionally, the number of iterations required during the training process decreased by 76.02% compared to DDQN.

Table 2: Results of Target Path Planning for a Single AGV

		DDQN	EKF-DDQN	PF-DDQN
Training Time		4.59 Hours	3.95 Hours	3.64 Hours
Solution Episode	After 56,568 episodes/(4.2 Hours)	After 16,482 episodes/(2.79 Hours)	After 13,564 episodes/(2.63 Hours)	
Target Hit Times	7,498	9,698	25,800	
Obstacle Hit Times	44,598	26,894	4,632	
Step-Time out Times	8,579	6,897	4,591	
Last Path Length	23 Grids	30 Grids	30 Grids	

Since there is only one AGV in this experiment, the constructed network model is relatively simple. Therefore, the PF-DDQN method is not significantly better than the EKF-DDQN method in terms of

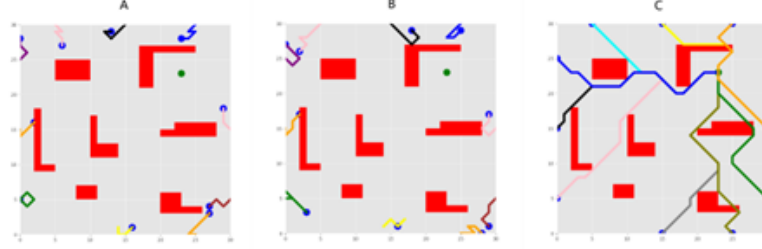


Figure 11: **Experiment 2 final path results of in A) DDQN, B) EKF-DDQN, and C) PF-DDQN after Multi AGVs path smoothing for 60000 episodes.**

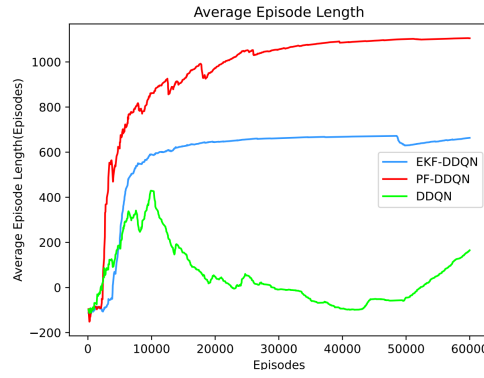


Figure 12: **For multi-AGV target path planning, the proposed method is compared with the learning curve after EKF-DDQN and DDQN training.**

final reward value. However, compared with PF-DDQN method, the reward curve of EKF-DDQN method has two big changes, which is about to fall into the local optimal solution, indicating that its stability is poor.

The proposed method minimizes unnecessary exploration by the AGV to a great extent by introducing the Particle Filter (PF) in the process of obtaining target network parameters. This reduces errors resulting from imprecise weight estimates through iterative refinement. Unlike DDQN, this method treats imprecise weights as state variables in the state-space equation, allowing it to converge to the correct range even if the previously learned network parameters are affected by errors. In comparison, DDQN exhibits a broader range of reward values and greater data fluctuations, making convergence less likely.

4.2 Experiment 2: Comparison of Path Planning for Multiple AGVs

In this experiment, the PF-DDQN, EKF-DDQN, and DDQN algorithms underwent 60,000 training iterations. Ten AGVs started their journeys from different fixed positions on the map, navigating through seven clusters of obstacles to reach designated fixed positions in the upper-right corner.

Figure 11 illustrates the paths planned by the three methods. It is evident from the figure that the algorithm proposed in this study successfully enables all AGVs to reach their target points, whereas the EKF-DDQN and DDQN algorithms did not achieve the same level of success.

The learning curves of the three methods are depicted in Figure 12. The experimental results demonstrate that the improved method exhibits faster convergence compared to the other two methods, with higher values achieved after convergence.

Table 3 presents the specific numerical simulation results of this experiment. From the table, it is observed that the DDQN and EKF-DDQN methods enabled the first AGV to reach the target after 16,987 and 27,721 training iterations, respectively. However, when multiple AGVs are involved, the

disturbance caused by the neural network's high variance increases exponentially, leading to a rapid decrease in learning efficiency.

As a result, the DDQN method requires a significant amount of time to forget the states associated with individual AGVs receiving high rewards. Conversely, the EKF-DDQN method, due to its highly nonlinear nature, experiences a decrease in accuracy, preventing all AGVs from reaching their target points as intended.

Table 3: Results of target path planning for a single AGV

DDQN Algorithm (Training Time: 5.14 Hours)				
AGV Index	Episode	Training Time	Last Path Length	Length To Best Result
AGV_1	17989	1.3H	87	24
AGV_2	—	—	—	24
AGV_3	—	—	—	18
AGV_4	—	—	—	14
AGV_5	—	—	—	8
AGV_6	—	—	—	26
AGV_7	—	—	—	24
AGV_8	—	—	—	22
AGV_9	—	—	—	18
AGV_10	—	—	—	9
EKF-DDQN Algorithm (Training Time: 5.74 Hours)				
AGV Index	Episode	Training Time	Last Path Length	Length To Best Result
AGV_1	27721	3.3H	27	24
AGV_2	—	—	—	24
AGV_3	—	—	—	18
AGV_4	—	—	—	14
AGV_5	—	—	—	8
AGV_6	—	—	—	26
AGV_7	—	—	—	24
AGV_8	—	—	—	22
AGV_9	—	—	—	18
AGV_10	—	—	—	9
PF-DDQN Algorithm (Training Time: 2.98 Hours)				
AGV Index	Episode	Training Time	Last Path Length	Length To Best Result
AGV_1	6584	0.96H	24	24
AGV_2	4783	0.67H	24	24
AGV_3	5869	0.72H	18	18
AGV_4	6202	0.78H	14	14
AGV_5	6563	0.81H	8	8
AGV_6	5905	0.73H	26	26
AGV_7	5968	0.74H	24	24
AGV_8	6330	0.79H	22	22
AGV_9	6097	0.76H	18	18
AGV_10	5780	0.71H	9	9

In contrast, the PF-DDQN algorithm proposed in this study successfully enables all AGVs to reach their target points. The algorithm converges faster and achieves better results in terms of the path lengths. The training time for the PF-DDQN algorithm is significantly less compared to the other two methods.

In conclusion, the PF-DDQN algorithm outperforms the DDQN and EKF-DDQN algorithms in terms of multi-AGV path planning. It exhibits faster convergence, higher accuracy, and better performance in terms of path lengths.

5 Conclusion

To summarize, this study introduces the PF-DDQN method for path planning involving multiple AGVs, which incorporates particle filtering. This approach addresses the limitations of the classical DDQN learning algorithm in noisy and complex environments, while also demonstrating superior fitting accuracy for complex models compared to the use of Kalman filtering.

The method utilizes a nonlinear model within a neural network to describe the system and integrates particle filtering to estimate the system's state. At each time step, the particle filter updates the state estimate based on current measurements, while the neural network enhances the accuracy of the estimation. By leveraging the neural network's ability to learn complex patterns in the environment and combining them with the state estimation from particle filtering, the proposed method offers an efficient and effective solution for path planning.

Simulation experiments were conducted to evaluate the performance of the method, revealing significant improvements in training time and path quality compared to the DDQN method, with respective enhancements of 92.62% and 76.88%. This research provides valuable insights into path planning and presents a novel and efficient solution applicable to multi-AGV path planning in complex environments. The findings hold promising potential for various applications, including robotics, autonomous vehicles, and unmanned aerial vehicles.

References

- [1] Yin, J., Li, L., Mourelatos, Z. P., et al. Reliable Global Path Planning of Off-Road Autonomous Ground Vehicles Under Uncertain Terrain Conditions. *IEEE Transactions on Intelligent Vehicles* 2023, IEEE.
- [2] Yin, J., Hu, Z., Mourelatos, Z. P., et al. Efficient Reliability-Based Path Planning of Off-Road Autonomous Ground Vehicles Through the Coupling of Surrogate Modeling and RRT. *IEEE Transactions on Intelligent Transportation Systems* 2023, IEEE.
- [3] Jones, M., Djahel, S., Welsh, K. Path-planning for unmanned aerial vehicles with environment complexity considerations: A survey. *ACM Computing Surveys* 2023, 55(11), 1-39.
- [4] Wu, Z., Dai, J., Jiang, B., et al. Robot path planning based on artificial potential field with deterministic annealing. *ISA Transactions* 2023, 138, 74-87.
- [5] Yao, M., Deng, H., Feng, X., et al. Improved dynamic windows approach based on energy consumption management and fuzzy logic control for local path planning of mobile robots. *Computers & Industrial Engineering* 2024, 187, 109767.
- [6] Sun, P. Z., Yang, Q., Kuang, W. J., et al. Limits on gas impermeability of graphene. *Nature* 2020, 579(7798), 229-232.
- [7] Aslan, M. F., Durdu, A., Sabanci, K. Goal distance-based UAV path planning approach, path optimization and learning-based path estimation: GDRRT*, PSO-GDRRT* and BiLSTM-PSO-GDRRT. *Applied Soft Computing* 2023, 137, 110156.
- [8] Mumtaz, J., Minhas, K. A., Rauf, M., et al. Solving Line Balancing and AGV Scheduling Problems for Intelligent Decisions using a Genetic-Artificial Bee Colony Algorithm. *Computers & Industrial Engineering* 2024, 109976.
- [9] Xin, B., Lu, S., Wang, Q., et al. Simultaneous Scheduling of Processing Machines and Automated Guided Vehicles via a Multi-View Modeling-Based Hybrid Algorithm. *IEEE Transactions on Automation Science and Engineering* 2023.
- [10] Zhang, L., Yan, Y., Hu, Y. Deep reinforcement learning for dynamic scheduling of energy-efficient automated guided vehicles. *Journal of Intelligent Manufacturing* 2023, 1-14.
- [11] Zhang, L., Yang, C., Yan, Y., et al. Automated guided vehicle dispatching and routing integration via digital twin with deep reinforcement learning. *Journal of Manufacturing Systems* 2024, 72, 492-503.

- [12] Liu, Y., Ping, Y., Zhang, L., et al. Scheduling of decentralized robot services in cloud manufacturing with deep reinforcement learning. *Robotics and Computer-Integrated Manufacturing* 2023, 80, 102454.
- [13] Chung, J., Fayyad, J., Younes, Y. A., et al. Learning team-based navigation: a review of deep reinforcement learning techniques for multi-agent pathfinding. *Artificial Intelligence Review* 2024, 57(2), 41.
- [14] Aradi, S. Survey of deep reinforcement learning for motion planning of autonomous vehicles. *IEEE Transactions on Intelligent Transportation Systems* 2020, 23(2), 740-759.
- [15] Huang, H., Savkin, A. V., Huang, C. Reliable path planning for drone delivery using a stochastic time-dependent public transportation network. *IEEE Transactions on Intelligent Transportation Systems* 2020, 22(8), 4941-4950.
- [16] Aggarwal, S., Kumar, N. Path planning techniques for unmanned aerial vehicles: A review, solutions, and challenges. *Computer Communications* 2020, 149, 270-299.
- [17] Li, X. S., Xu, C. G., Zhang, Y., et al. Investigation into gas production from natural gas hydrate: A review. *Applied Energy* 2016, 172, 286-322.
- [18] Sekander, S., Tabassum, H., Hossain, E. Multi-tier drone architecture for 5G/B5G cellular networks: Challenges, trends, and prospects. *IEEE Communications Magazine* 2018, 56(3), 96-103.
- [19] Huang, Z., Zhu, D., Sun, B. A multi-AUV cooperative hunting method in 3-D underwater environment with obstacle. *Engineering Applications of Artificial Intelligence* 2016, 50, 192-200.
- [20] Li, G., Liu, C., Wu, L., et al. A mixing algorithm of ACO and ABC for solving path planning of mobile robot. *Applied Soft Computing* 2023, 148, 110868.
- [21] Li, B., Qi, X., Yu, B., et al. Trajectory planning for UAV based on improved ACO algorithm. *IEEE Access* 2019, 8, 2995-3006.
- [22] Patle, B. K., Pandey, A., Parhi, D. R. K., et al. A review: On path planning strategies for navigation of mobile robot. *Defence Technology* 2019, 15(4), 582-606.
- [23] Mnih, V., Kavukcuoglu, K., Silver, D., et al. Human-level control through deep reinforcement learning. *Nature* 2015, 518(7540), 529-533.
- [24] Van Hasselt, H., Guez, A., Silver, D. Deep reinforcement learning with double q-learning. In *Proceedings of the AAAI conference on artificial intelligence* 2016, 30(1).
- [25] Hessel, M., Modayil, J., Van Hasselt, H., et al. Rainbow: Combining improvements in deep reinforcement learning. In *Proceedings of the AAAI conference on artificial intelligence* 2018, 32(1).
- [26] Igl, M., Zintgraf, L., Le, T. A., et al. Deep variational reinforcement learning for POMDPs. In *International Conference on Machine Learning* 2018, 2117-2126.
- [27] Naesseth, C., Linderman, S., Ranganath, R., et al. Variational sequential monte carlo. In *International conference on artificial intelligence and statistics* 2018, 968-977.
- [28] Gregor, K., Danihelka, I., Graves, A., et al. DRAW: A recurrent neural network for image generation. In *International conference on machine learning* 2015, 1462-1471.
- [29] Rico Jonschkowski, Divyam Rastogi and Oliver Brock. Differentiable Particle Filters: End-to-End Learning with Algorithmic Priors, 2018; arXiv:1805.11122.
- [30] Siqi Liu, Guy Lever, Zhe Wang, Josh Merel, S. M. Ali Eslami, Daniel Hennes, Wojciech M. Czarnecki, Yuval Tassa, Shayegan Omidshafiei, Abbas Abdolmaleki, Noah Y. Siegel, Leonard Hasenclever, Luke Marris, Saran Tunyasuvunakool, H. Francis Song, Markus Wulfmeier, Paul Muller, Tuomas Haarnoja, Brendan D. Tracey, Karl Tuyls, Thore Graepel and Nicolas Heess. From Motor Control to Team Play in Simulated Humanoid Football, 2021;

- [31] Ma, M., Mao, Z. Deep-convolution-based LSTM network for remaining useful life prediction. *IEEE Transactions on Industrial Informatics* 2020, 17(3), 1658-1667.
- [32] Muruganantham, A., Tan, K. C., Vadakkepat, P. Evolutionary dynamic multiobjective optimization via Kalman filter prediction. *IEEE Transactions on Cybernetics* 2015, 46(12), 2862-2873.
- [33] Gao, X., Luo, H., Ning, B., et al. RL-AKF: An adaptive Kalman filter navigation algorithm based on reinforcement learning for ground vehicles. *Remote Sensing* 2020, 12(11), 1704.
- [34] Zhengxin, J., Qin, S., Yujiang, W., et al. An Immune Genetic Extended Kalman Particle Filter approach on state of charge estimation for lithium-ion battery. *Energy* 2021, 230, 120805.
- [35] Korkin, R., Oseledets, I., Katrutsa, A. Multiparticle Kalman filter for object localization in symmetric environments. *Expert Systems with Applications* 2024, 237, 121408.